Long-Residency Hydration, Cation Binding, and Dynamics of Loop E/Helix IV rRNA-L25 Protein Complex

Kamila Réblová,* Nad'a Špačková,† Jaroslav Koča,* Neocles B. Leontis,‡ and Jiří Šponer†§

*National Centre for Biomolecular Research, Faculty of Sciences, Masaryk University, Kotlářská 2, 61137 Brno, Czech Republic; †Institute of Biophysics, Academy of Sciences of the Czech Republic, Královopolská 135, 61265 Brno, Czech Republic; ‡Chemistry Department and Center for Biomolecular Sciences, Bowling Green State University, Bowling Green, Ohio 43403; and §Institute of Organic Chemistry and Biochemistry, Academy of Sciences of the Czech Republic, Flemingovo n. 2, 16610 Prague, Czech Republic

ABSTRACT Molecular dynamics simulations of RNA-protein complex between *Escherichia coli* loop E/helix IV (LE/HeIV) rRNA and L25 protein reveal a qualitative agreement between the experimental and simulated structures. The major groove of LE is a prominent rRNA cation-binding site. Divalent cations rigidify the LE major groove geometry whereas in the absence of divalent cations LE extensively interacts with monovalent cations via inner-shell binding. The HeIV region shows bistability of its major groove explaining the observed differences between x-ray and NMR structures. In agreement with the experiments, the simulations suggest that helix-α1 of L25 is the least stable part of the protein. Inclusion of Mg^{2+} cations into the simulations causes perturbation of basepairing at the LE/HeIV junction, which does not, however, affect the protein binding. The rRNA-protein complex is mediated by a number of highly specific hydration sites with long-residing water molecules and two of them are bound throughout the entire 24-ns simulation. Long-residing water molecules are seen also outside the RNA-protein contact areas with water-binding times substantially enhanced compared to simulations of free RNA. Long-residency hydration sites thus represent important elements of the three-dimensional structure of rRNA.

INTRODUCTION

The recently determined atomic-resolution structures of ribosomal subunits confirm that the ribosomal RNA (rRNA) molecules (5S, 16S, and 23S) comprise short regions formed by Watson-Crick basepairs and so-called RNA motifs, i.e., specific non-Watson-Crick basepaired regions (Ban et al., 2000; Wimberly et al., 2000). Recurrent, modular RNA motifs represent key structural elements in the ribosome (Leontis and Westhof, 1998b, 2003; Moore, 1999). Studies of RNA motifs and their molecular interactions in the ribosome are thus important to understand fundamental aspects of ribosomal structure and function. Available crystal structures of ribosomal subunits (Ban et al., 2000; Harms et al., 2001; Wimberly et al., 2000; Yusupov et al., 2001) and smaller RNA-protein complexes (Agalarov et al., 2000; Lu and Steitz, 2000; Nikulin et al., 2003; Perederina et al., 2002; Wimberly et al., 1999) reveal a wide repertoire of different types of molecular interactions.

Modern computational methods represent an important tool that can complement experiments and provide additional information about structure, dynamics, and molecular recognition of nucleic acids and proteins (Auffinger and Westhof, 1998, 1999; Beaurain and Laguerre, 2003; Correll et al., 1997; Hermann et al., 1998; Cheatham and Young, 2000; Norberg and Nilsson, 2002; Orozco et al., 2003; Reblova et al., 2003a,b; Sarzynska et al., 2000; Schneider et al., 2001; Zacharias, 2000). In the previous study (Reblova et al., 2003b) we have investigated the 5S rRNA loop E (LE) secondary motif of *Escherichia coli* and spinach chloroplast utilizing molecular dynamics (MD) simulations with explicit inclusion of solvent and counterions. The bacterial loop E forms a unique duplex architecture due to seven consecutive non-Watson-Crick basepairs and is involved in both RNA-RNA and RNA-protein interactions. The simulations indicate that the LE could serve as a rigid docking segment recognized by other ribosomal elements. LE has a unique capability to extensively bind monovalent and divalent cations in the deep major groove (Auffinger et al., 2003, 2004a; Lu and Steitz, 2000). We employed RNA motif analysis and simulations to predict that the bacterial and spinach chloroplast LE regions, despite pronounced sequence variability, adopt nearly isosteric geometries (Leontis and Westhof, 1998a), which is also confirmed by independent NMR study (Vallurupalli and Moore, 2003). The simulations suggest that the unique LE architecture is complemented by several highly specific hydration sites with long-residency water molecules that are not seen in regular RNA duplexes (Reblova et al., 2003b).

Ribosomal RNA-protein complexes are essential in many biological processes and are intensely studied by experimental and computational methods. The complex of loop E and the ribosomal L25 protein is one of the best-characterized RNA-protein complexes (Lu and Steitz, 2000; Stoldt et al., 1999). The biological role of L25 is yet to be established. The L25 protein does not appear to be conserved in all bacterial ribosomes and has no counterpart in archaea or eukarya (Nevskaya et al., 2000). On the other hand its extensive interactions with 5S rRNA LE region and with the adjacent helix IV (HeIV) of 5S rRNA are quite specific indicating that it has some biological roles. Furthermore, such specific

Submitted June 4, 2004, and accepted for publication August 26, 2004.

Address reprint requests to Jiří Šponer, E-mail: sponer@ncbr.chemi.muni.cz.

0006-3495/04/11/3397/16 $2.00

doi: 10.1529/biophysj.104.047126

molecular interactions represent a challenge for structural studies. Although there is no x-ray structure available for the large ribosomal subunit of *E. coli*, our preliminary docking using x-ray structure of the 50S subunit of *Haloarcula marismortui* (not shown) in fact suggests that the second A-stack region of bacterial loop E could interact with the A-site finger in 23S rRNA whereas the first A-stack interacts with L25 and is outside the ribosome. Then L25 could, for example, play a role in supporting the *E. coli* loop E (keeping it well organized) so that it can interact with the A-site finger and couple motions of the L9 domain with the A-site finger. Both L9 domain and A-site finger make bridges to the 30S subunit and move during translocation. It is notable that 5S rRNA has been implicated in translocation.

The non-Watson-Crick LE basepairs provide a highly sequence-specific hydrogen-bonding surface in the minor groove recognized by the L25 protein. Furthermore, the non-Watson-Crick basepairs confer considerable plasticity to the RNA helix, which becomes more accessible to the protein. The structure of the bacterial complex of loop E/helix IV and ribosomal L25 protein (LE/HeIV-L25) has been determined by NMR spectroscopy and x-ray crystallography (Lu and Steitz, 2000; Stoldt et al., 1999). Free LE/HeIV rRNA and free L25 protein have also been studied (Correll et al., 1997; Stoldt et al., 1998). LE and HeIV establish distinct interactions with L25, as evidenced by both x-ray and NMR complexes (Figs. 1–3). The bacterial LE motif contains two A104-A73 and A99-A78 cross-strand adenine stacks (Fig. 1 *a*) that significantly distort the sugar-phosphate backbone and narrow the LE major groove. The adjacent HeIV contains two wobble basepairs forming G96-G81 cross-strand guanine stack (Fig. 1 *a*). The major (deep) groove width of HeIV is enlarged relatively to Watson-Crick A-RNA duplex due to A99-A78 and G96-G81 cross-strand purine stacks.

The x-ray structures of the LE/HeIV-L25 complex (Nucleic Acid Database (NDB) code, PR0018) and of the free LE/HeIV fragment (NDB code, URL069) reveal several magnesium ions bound via inner-shell and outer-shell binding (Correll et al., 1997; Lu and Steitz, 2000). As discussed recently, magnesium cations can be occasionally misassigned in experimental structures and some of them may correspond to anion-binding positions, water molecules, or two closely spaced cations representing a single alternating binding site (Auffinger et al., 2004b). Qualitative geometrical criteria to identify such suspicious binding sites were suggested (Auffinger et al., 2004b). Based on these criteria the x-ray structure of the complex does not show any Mg^{2+} ions that could correspond to anions but there are two ions that likely represent a single species. The x-ray structure of the free RNA reveals one suspicious Mg^{2+} ion (binding site at G100) in the minor groove of LE (see below).

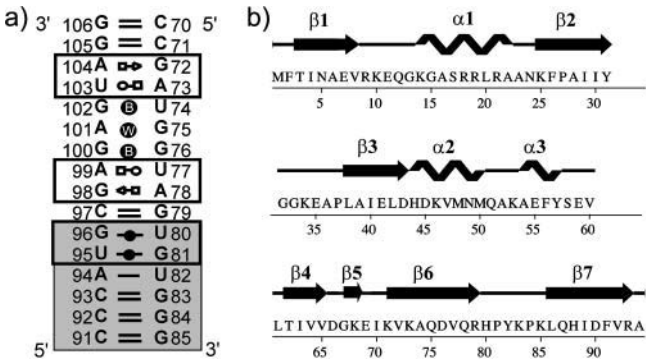

FIGURE 1 (*a*) Sequence of the studied LE/HeIV RNA duplex. The HeIV part is in shaded field; two A-stacks and one G-stack are in black boxes. Symbols identify non-Watson-Crick basepairs (Leontis et al., 2002). (*b*) Schematic arrangement of secondary structures of the ribosomal L25 protein; the numbers correspond to the individual protein residues.

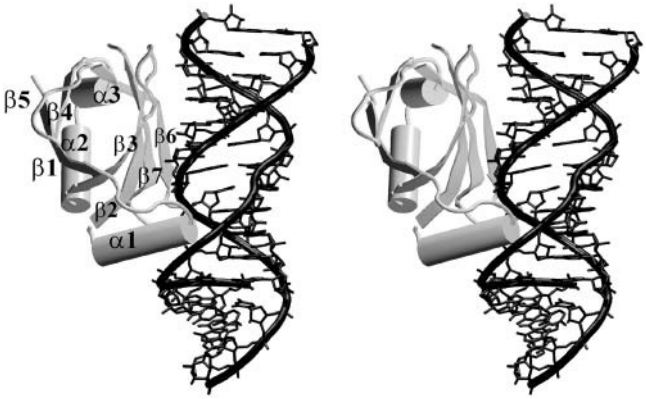

FIGURE 2 Stereo view of the x-ray LE/HeIV-L25 complex (NDB code, PR0018); secondary elements of L25 protein are marked.

The L25 protein is composed of a seven-stranded closed β-barrel (strands $\beta1$–$\beta7$) and three α-helices ($\alpha1$–$\alpha3$) (Figs. 1 *b* and 2) (Lu and Steitz, 2000; Stoldt et al., 1999). The strands $\beta2$, $\beta3$, $\beta6$, $\beta7$, and the helix-$\alpha1$ interact with the LE/HeIV fragment (Fig. 2) via two distinct contact areas. While the antiparallel β-ribbons ($\beta2$, $\beta3$, $\beta6$, $\beta7$) interact with the minor groove of LE (LE contact area), the N-terminal tip of the helix-$\alpha1$ interacts with the widened major groove of HeIV (Lu and Steitz, 2000; Stoldt et al., 1999) (HeIV contact area). There are multiple direct H-bonds between amino acids and bases in the two contact areas. The x-ray structures reveal that the LE/HeIV geometry is largely unaffected upon binding of L25, with the most significant change being a marked narrowing of the major groove of HeIV by ~5 Å (Fig. 3, *a* and *b*) (Correll et al., 1997; Lu and Steitz, 2000). Bound LE/HeIV fragment thus shows a geometry that we call ''closed geometry'' throughout this study whereas the uncomplexed LE/HeIV fragment shows ''open geometry'' of the major groove of HeIV (Correll et al., 1997; Lu and Steitz, 2000). Helix-$\alpha1$ (residues 14–22) of isolated L25 is unstructured in solution (Stoldt et al., 1998). The experimental data suggest that the recognition of L25 protein by LE/HeIV rRNA is mediated by two preformed recognition elements, i.e., the β-sheet surface of L25 and the widened

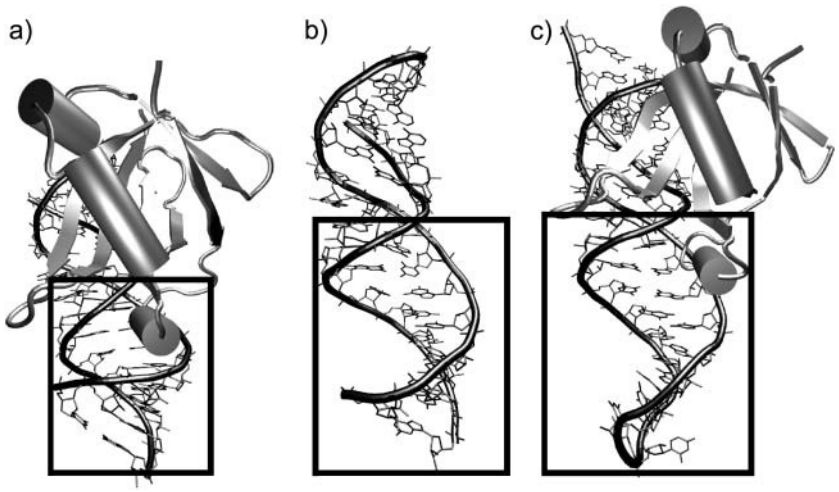

FIGURE 3 Experimental structures of the LE/HeIV-L25 complex and the free LE/HeIV fragment. (*a*) X-ray LE/HeIV-L25 complex with narrow major groove of HeIV (closed geometry) (NDB code, PR0018). (*b*) X-ray structure of free LE/HeIV fragment with wider major groove of HeIV (open geometry) (NDB code, URL069). (*c*) NMR LE/HeIV-L25 complex with wider major groove of HeIV (open geometry) (Protein Data Bank (PDB) code, 1D6K). HeIV is inside the black box.

minor groove of LE (Stoldt et al., 1998, 1999). In the course of intermolecular recognition, the helix-α1 is structured and turns toward the more flexible major groove of HeIV, where it inserts the side chains of its N-terminal tip and anchors the structure of the complex (Fig. 2) (Stoldt et al., 1998). Comparison of NMR and x-ray LE/HeIV-L25 complexes reveals several congruencies and discrepancies. Differences in experimental conditions used in the respective x-ray and NMR studies are listed in the Supplementary Material. The NMR structure shows several direct intermolecular H-bonds (Asp^{90}-G75, His^{88}-G75, Arg^{9}-G76) also observed in the x-ray structure (Lu and Steitz, 2000) but there are other potential contacts that could not be determined with certainty (Stoldt et al., 1999). Furthermore, the x-ray structure describes direct H-bonds between Lys^{14} and U80, between Lys^{14} and G79, and between Gln^{78} and G76. The geometry of LE predicted by NMR appears to be identical with the x-ray structure but there is an apparent difference in NMR and x-ray geometries of HeIV (Fig. 3, *a* and *c*). The major groove of HeIV is widened in the NMR complex by ~5–7 Å in comparison with the x-ray structure and actually resembles the open geometry of the free x-ray LE/HeIV fragment (Fig. 3).

We employed molecular dynamics (MD) to study the LE/HeIV-L25 complex. Our results provide details of the molecular interactions that explain some of the structural differences between the NMR and x-ray structures and give an additional detailed insight into the molecular interactions. Specifically, the simulations suggest the crucial role of tightly bound water molecules in ribosomal assemblies. The residency times of water molecules in selected hydration sites in the presently investigated complex are longer than in any MD study reported so far for nucleic acids, being up to two orders of magnitude longer than in common DNA and RNA hydration sites.

MATERIALS AND METHODS

Starting structures

The *E. coli* ribosomal complex LE/HeIV-L25 was taken from x-ray data (NDB code, PR0018; 1.8-Å resolution) (Lu and Steitz, 2000). The packing interactions of the molecule in the asymmetric unit between RNA and adjacent proteins involve the top and bottom parts of the RNA, however, no protein-protein contacts were detected. The structure contains 94 residues of the L25 protein, 36 residues of the LE/HeIV fragment, and five Mg^{2+} ions. Four terminal unpaired bases at the ends were omitted. We carried out two simulations of the LE/HeIV-L25 complex, ''COM1'' (24 ns) with inclusion of five Mg^{2+} ions and ''COM2'' (11 ns) in the absence of Mg^{2+} ions (Table 1). Furthermore, we performed simulations of the individual components of the complex starting again from the same crystal structure. The LE/HeIV fragment was simulated with five Mg^{2+} ions (simulation ''RNA1''; 14.5 ns) and the L25 protein was simulated for 10 ns (simulation ''PROT1'') (Table 1). A further simulation of the L25 protein ''PROT2'' (19 ns) was run at elevated temperature (400 K) to enhance the sampling. Moreover, the uncomplexed LE/HeIV fragment was also taken from the x-ray data (NDB code, URL069; 3.0-Å resolution) and was simulated for 18 ns (simulation

TABLE 1 Summary of the simulations carried out in this article

Starting structure (NDB code)	Simulated system	Name of the simulation	Length of the simulation (ns)	Presence of ions
PR0018	LE/HeIV-L25 complex	COM1	24	5 Mg^{2+}, 15 Na^{+}
PR0018	LE/HeIV-L25 complex	COM2	11	25 Na^{+}
PR0018	L25 protein	PROT1	10	5 Cl^{-}
PR0018	L25 protein	PROT2*	19	5 Cl^{-}
PR0018	LE/HeIV RNA	RNA1	14.5	5 Mg^{2+}, 20 Na^{+}
URL069	LE/HeIV RNA	RNA2	18	5 Mg^{2+}, 20 Na^{+}

*Simulation at 400 K.

''RNA2'') with five Mg^{2+} ions adopting a similar arrangement as in the LE/HeIV-L25 complex (Correll et al., 1997). The sequence of the uncomplexed LE/HeIV fragment used in the simulation was identical to the LE/HeIV fragment in the complex (Fig. 1 *a*).

The simulations were carried out using the AMBER-6.0 program (Pearlman et al., 1995) with the Cornell et al. force field (Cornell et al., 1995). The RNA molecules were neutralized by sodium counterions initially placed by the Xleap module of AMBER-6.0 at the most negative positions close to the RNA whereas Mg^{2+} ions were placed based on the x-ray structures. In case of the low-resolution x-ray structure of the free LE/HeIV fragment, the x-ray Mg^{2+} cation distribution was somewhat modified, to make it similar to the distribution seen in the complex. The x-ray structure of the free LE/HeIV fragment contains eight Mg^{2+} ions, six of them bound in the area of LE/HeIV. Five Mg^{2+} ions bound in the major groove of LE and HeIV were rearranged to mimic the Mg^{2+}-binding positions in the LE/HeIV-L25 x-ray structure. Nevertheless, as seen in Table 2, we could not achieve identical initial ion placement due to difference in starting solute geometries. As demonstrated below, it has some impact on the simulated structures. The sixth Mg^{2+} ion that is bound in the minor groove of LE at G100 was omitted. This cation can actually be mislabeled and may even correspond to an anion-binding position, as discussed in the literature (Auffinger et al., 2004b). The remaining two divalent cations not interacting with the major groove were also omitted.

Cl^- ions were used in simulations PROT1 and PROT2 for neutralization of the protein and their initial positions were suggested by Xleap. The following parameters were used: Na^+ radius 1.868 Å and well depth 0.00277 kcal/mol, Mg^{2+} radius 0.7926 Å and well depth 0.8947 kcal/mol, and Cl^- radius 1.948 Å and well depth 0.265 kcal/mol (Ross and Hardin, 1994). The limitations imposed by the simple force-field description of ions were briefly discussed in our preceding study (Reblova et al., 2003b). The polar hydrogens of the protein were added and protonation states of all histidines in the LE/HeIV-L25 complex were set to allow formation of proper H-bonds. Thus all three histidines were (δ protonated (Amber code HID)). Crystal water molecules were used in the simulation start and a cubic box of the TIP3P water molecules was added around the RNA to a depth of 12 Å on each side of the solute. The Sander module of AMBER-6.0 was used for all minimizations and molecular dynamics simulations. All residues were restrained by force constants, which were gradually reduced from 500 to 0 kcal/mol in the course of 5000 steps while the rest of the system was allowed to relax. The systems were then heated from 50 K up to 300 K in 100 ps. The production runs were carried out at 300 K with constant-pressure boundary conditions and the particle-mesh Ewald (PME) method using Berendsen temperature coupling algorithm (with a time constant of 0.2 ps) (York et al., 1993). One simulation (see above) was carried out at elevated temperature (400 K) to enhance sampling. For this simulation, the system was gradually heated from 300 K to 400 K during the first 100 ps using NPT conditions (constant pressure ensemble). The production run was then continued at 400 K using NVT (constant volume ensemble). The NVT simulations imply high pressure that may artificially stabilize the structure (Zhou et al., 2001). The outcome of the elevated temperature simulations is also limited by the fact that at elevated temperature the system is not represented by a Boltzmann distribution equivalent to prolongation of a room temperature simulation. Nonetheless, elevated temperature simulations often provide insights into labile parts of the simulated structures. The center of mass velocity was periodically removed during the production dynamics (Harvey et al., 1998). Trajectories were analyzed using the Carnal module of AMBER and structures were visualized using VMD (molecular visualization program, http://www.ks.uiuc.edu/research/vmd/) (Humphrey et al., 1996). Hydration and distribution of ions were calculated with the Ptraj module of the AMBER-6.0 and visualized using UCSF MidasPlus (University of California, San Francisco, CA) (Ferrin et al., 1988). Systematic monitoring of the solute-to-water distances was carried out using the Carnal module of AMBER. All direct solute-solvent contacts were detected during the whole simulation and then analyzed in detail. To obtain some crude estimate of the energetics, energy analysis was carried out using the Anal module of AMBER to evaluate energetic contributions between individual residues of the protein and the LE/HeIV fragment. Electrostatic (E_{el}) and van der Waals (E_{vdw}) nonbonding interactions between individual residues were extracted from the equation describing the molecular mechanics energy:

$$E_{MM} = E_{bond} + E_{angle} + E_{tors} + E_{vdw} + E_{el}.$$

The E_{vdw} interactions were described by Lennard-Jones potential whereas the E_{el} interactions were described by Coulomb term. E_{vdw} and E_{el} interactions were computed between RNA and protein residues forming intermolecular H-bonds and the values of energetic contributions were averaged along the trajectory. The charges of the residues were not modified after the dissection and the energy calculations were carried out assuming a dielectric constant of 1. Thus, the interaction energies provide only a very crude insight in the stability because solvent screening is not included. The DO_DSSP module of the GROMACS-2.0 program was used for analysis of the secondary structure elements of the protein (van der Spoel et al., 1999).

TABLE 2 Comparison of Mg^{2+} positions in the course of RNA2 and COM1 simulations (see the text)

Mg^{2+} ion	Simulation RNA2	Simulation COM1
A	G105(O2P) Inner-shell binding	G106(O6,O2P) and G105(O2P) Outer-shell binding
B	A101(O2P) Inner-shell binding	G98(O2P), C97(O2P) and Gln^{12}(O) Outer-shell binding
C	U74(O2P) and A99(O2P) Inner-shell binding	G100(O2P) Inner-shell binding
D	G75(O1P) Inner-shell binding	U74(O2P), G75(O2P) and A99(O2P) Outer-shell binding
E	C93(O2P) Inner-shell binding	U95(O4) and G96(O6) Inner-shell binding

All Mg^{2+} ions were stable in the course of the simulations except Mg^{2+} ion B in COM1 simulation. Mg^{2+} ion B was involved in outer-shell binding to G98(O2P), C97(O2P), and Gln^{12}(O) after 20 ns of the simulation COM1.

RESULTS

Molecular dynamics of the LE/HeIV-L25 complex

We have carried out 24-ns simulation of the LE/HeIV-L25 complex in the presence of Mg^{2+} (simulation COM1). The root-mean-square deviation (RMSD) value with respect to the x-ray structure was 2.3 ± 0.5 Å (see Fig. S1 in Supplementary Material). This is a very low RMSD value, considering the size of the simulated system, indicating that the system is very close to the starting x-ray geometry and rather rigid. The RMSD between the averaged MD structure in the time period of 19–24 ns and the x-ray structure is ~1.7 Å. The Supplementary Material section presents selected PDB files illustrating this as well as the subsequent simulations. The complete trajectories may be obtained from the authors upon request.

LE and HeIV reveal distinct major groove dynamics

The geometry of LE did not show any significant changes in the course of the simulation. Minor fluctuations of the major groove width were observed in the range of 1–2 Å relative to the starting x-ray structure (see Table S1 in Supplementary

Material). In contrast, the adjacent HeIV region showed considerable fluctuations of the major groove with oscillations in the range of 3–5 Å in the course of the simulation. In the initial time period of 0–7.5 ns the major groove width of HeIV showed no dynamics and structural changes. Its geometry corresponded to the closed geometry of the x-ray LE/HeIV-L25 complex with interphosphate distances in the range of 12–14 Å. In the time period of 7.5–15 ns we observed widening of the major groove of HeIV, resembling the open geometry of free LE/HeIV fragment (Correll et al., 1997) with interphoshate distances in the range of 16–18 Å. The HeIV major groove closed again during the time period of 15–24 ns, essentially reestablishing the x-ray geometry (supplementary Table S1; Fig. 4). These dynamic changes thus illustrate widening and narrowing of the major groove of HeIV in the course of the simulation (supplementary Table S1; Fig. 4). We calculated histograms for the major groove widths. Although a single state was identified for the major groove width of LE with averaged value of 8.8 Å, two distinct substates were seen for the HeIV with averaged values of 14.5 Å (closed geometry) and 16.7 Å (open geometry) (Fig. 5).

Perturbation of basepairing at the LE/HeIV junction

The majority of basepairs were remarkably stable and were in agreement with the x-ray structure, except for the three consecutive *cis*-Watson-Crick/Watson-Crick basepairs at the LE/HeIV junction. The standard G79=C97 basepair shows G79(N1)-C97(N3), G79(O6)-C97(N4), and G79(N2)-C97(O2) H-bonds. The first two H-bonds experienced two full disruption events during the time periods of 8.3–9.5 ns and 10.1–13.1 ns whereas the third H-bond fluctuated in these time periods. The U80/G96 basepair was initially stabilized by U80(N3)-G96(O6) and U80(O2)-G96(N1) H-bonds. After 2 ns of the simulation the U80 base adopted position out of plane of the basepair and oriented the U80(N3) atom directly against the G96(N1) atom, in a seemingly repulsive interaction. This geometry was observed until the end of simulation. It caused complete disruption of the original H-bonds while a new fluctuating H-bond between U80(O2) and G96(N2) was formed. The third G81/U95 basepair was initially stabilized by U95(O2)-G81(N1) and U95(N3)-G81(O6) H-bonds. The first H-bond showed fluctuations from 0 to 6 ns and from 15 to 24 ns around U95(O2)-G81(N1) distance of 3.5 Å. The second H-bond was disrupted in the course of the whole simulation. The crystal structure does not indicate any perturbation of these basepairs and, as explained below, we suggest that the perturbation of basepairing is due to inclusion of the nearby

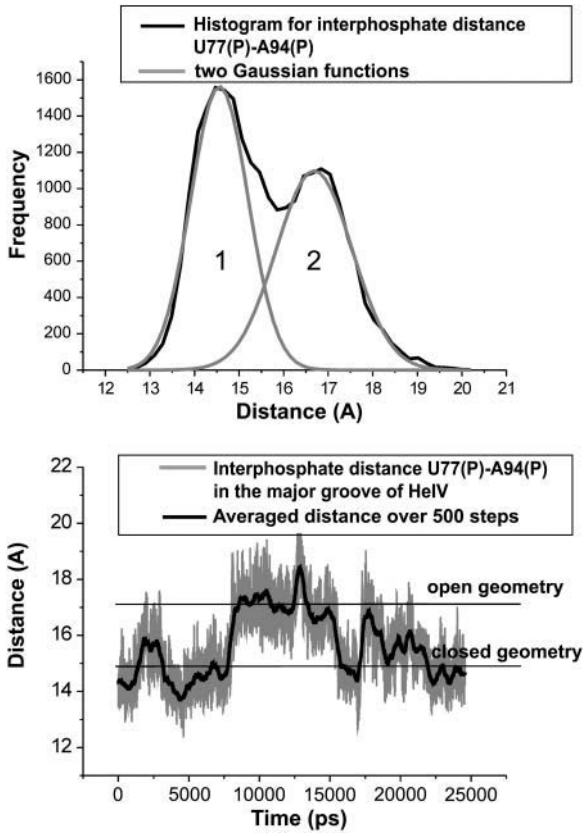

FIGURE 5 (*Top*) Histogram of the U77(P)-A94(P) interphosphate distance in the course of simulation decomposed by Gaussian functions. Two substates corresponding to the closed (*1*) and open geometry (*2*) were identified. (*Bottom*) Time course of the U77(P)-A94(P) distance.

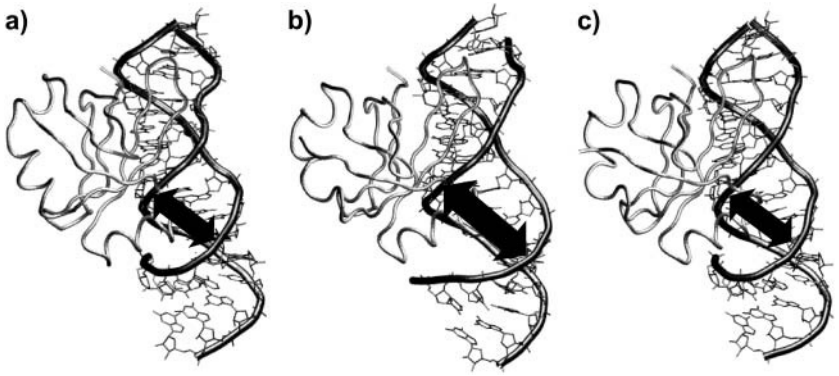

FIGURE 4 Averaged MD structures of the LE/HeIV-L25 complex in the presence of Mg^{2+} ions show different geometries of the major groove of HeIV on the nanosecond timescale. (*a*) Averaged structure in the time period 0–7.5 ns corresponds to the closed geometry. (*b*) Averaged structure in the time period 10–15 ns corresponds to the open geometry. (*c*) Averaged structure in the time period 20–24 ns corresponds to the closed geometry. Full set of interphosphate distances is listed in supplementary Table S1.

Mg^{2+} cation. Because the perturbation occurs outside the protein-binding area the protein binding seems to be unaffected.

L25 protein in LE/HeIV-L25 complex is rigid

The protein structure was not significantly modified in the course of the simulation compared with the x-ray starting geometry. The instantaneous RMSD value with respect to the x-ray structure was 2.3 ± 0.3 Å. The RMSD value of the protein backbone (calculated only for C_α atoms) with respect to the x-ray structure was 1.6 ± 0.3 Å. Secondary structures were monitored in the course of simulation. Modest structural change (turning) was observed for the helix-α2 (see Figs. S2 and S3 in Supplementary Material). This change was identified after 0.5 ns of the simulation and persisted until the end of the simulation (24 ns). The helix-α2 shows no contact with the LE/HeIV fragment and its modest structural change did not affect the stability of the LE/HeIV-L25 complex. Other secondary structure elements revealed no structural changes.

Intermolecular interactions between L25 and LE/HeIV are well preserved

The x-ray structure (Lu and Steitz, 2000) shows the following intermolecular H-bonds between amino acids and bases: G75(N2)-Asp^{90}(OD2), G76(N3)-Gln^{78}(NE2), G98(O6)-Lys^{14}(N), U80(O4)-Lys^{14}(NZ), and G79(N7)-Lys^{14}(NZ) (the third H-bond was not noticed in the original article but is evident in the structure). The first two interactions occur in the first contact area (LE) and require presence of specific non-Watson-Crick basepairs. The remaining three contacts are positioned in the second contact area (HeIV). All these H-bonds were observed in our simulation albeit some of them with occupancy below 100% (Fig. 6; Table 3). Numerous intermolecular H-bond contacts were identified between amino acids and sugar-phosphate backbone, again with reasonable agreement with the x-ray data. We monitored all intermolecular x-ray H-bonds and further analyzed all contacts seen with occupancy ≥35% in the simulation (Table 3). Individual intrinsic electrostatic (E_{el}) and van der Waals (E_{vdw}) interaction energies (see Materials and Methods) were calculated between residues on the RNA-protein interface that form H-bonds with occupancy ≥35% (see Table S2 in Supplementary Material). It is noted that these intrinsic interaction energies are calculated assuming single residues and relative dielectric constant of 1, and thus may differ significantly from the effective binding energies within the biomolecular environment. We observed that stable H-bonds (with occupancy 100%) were often accompanied by strong E_{el} interactions between oppositely charged residues (supplementary Table S2). Strong electrostatic interactions were mainly observed in the second contact area due to the presence of Lys^{14}, Arg^{18}, and Arg^{19} amino acids (supplementary Table S2). Furthermore, the experimental x-ray study (Lu and Steitz, 2000) describes one hydrophobic interaction between Pro^{37} and A73. The calculated value of the E_{vdw} energy of this contact is −1.2 ± 0.3 kcal/mol along the trajectory, i.e., an order of magnitude below van der Waals stacking energy between two consecutive basepairs in a regular double helix but comparable, e.g., to sugar-base stacking (Sponer et al., 1997). Due to the limitations stemming from the size of the complex, the presence of ions and formation of long-residing water bridges no free-energy calculations were attempted. However, we plan to carry out such calculations in the near future.

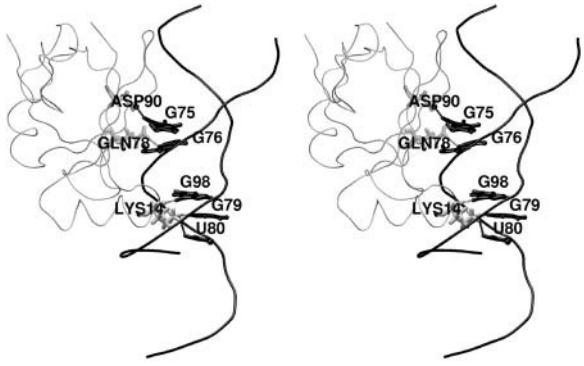

FIGURE 6 Stereo view of the LE/HeIV-L25 complex with H-bonds between amino acids and bases seen in the simulation.

The HeIV major groove dynamics affects the hydrogen bonding

Dynamic substates (open and closed geometry) of the major groove of HeIV are reflected by modest changes of the protein-binding pattern. All intermolecular amino-acid-base contacts were stable, however, several intermolecular contacts between amino acids and phosphate groups were disrupted. In the x-ray structure, Arg^{18} bridges opposite phosphate groups by forming Arg^{18}(NH2-HH21)-A78(O1P) and Arg^{18}(NH1-HH11)-C93(O2P) H-bonds (see Table 3). The Arg^{18}(NH1)-C92(O1P) distance is 3.2 Å but the corresponding hydrogen (NH1-HH12) does not appear to be properly oriented to form an H-bond. The Arg^{18}(NH1)-C92(O2P) distance is 3.9 Å. In the time period of 0–7.5 ns (closed geometry) we observed bifurcated interaction of Arg^{18}(NH1-HH12) with C92(O2P) and C92(O1P) that is not seen in the x-ray structure (see Fig. S4 *a* in Supplementary Material). Moreover, fluctuating Arg^{18}(NH2-HH22)-C92(O2P) H-bond (not seen in the x-ray structure) was noticed. Opening of the major groove (7.5–15 ns) increased the distance between the opposite phosphates in HeIV resulting in disruption of the Arg^{18}-C92 and Arg^{18}-C93 interactions whereas the Arg^{18}(NH2)-A78(O1P) H-bond persisted (supplementary Fig. S4 *b*). The contacts of the

TABLE 3 Direct intermolecular H-bonds with occupancy ≥35% between amino acids and bases and between amino acids and sugar-phosphate backbone

Amino acid(atom)-base(atom)	Occupancy (%)	X-ray distance (Å)	MD distance (Å)	SD (Å)
Gln^{78}(NE2)-G76(N3)	100	3.1	3.1	0.2
Asp^{90}(OD2)-G75(N2)	75	2.9	3.7	1.3
Lys^{14}(NZ)-G79(N7)	100	2.9	3.0	0.1
Lys^{14}(NZ)-U80(O4)	50	3.0	3.9	0.8
Lys^{14}(N)-G98(O6)	85	3.2	3.2	0.5
Amino acid(atom)-sugar-phosphate backbone(atom)				
Arg^{21}(NH2)-G76(O3′)	100	3.0	3.0	0.2
Gln^{78}(OE1)-G76(O2′)	98	2.7	2.8	0.4
Tyr^{31}(OH)-U103(O2′)	94	2.8	2.9	0.2
His^{88}(NE2)-G75(O2′)	95	3.5	3.1	0.4
Arg^{9}(NH1)-G76(O2P)	100	2.8	2.8	0.1
Arg^{21}(NH1)-U77(O1P)	100	2.9	2.7	0.1
Gly^{13}(N)-G76(O1P)	95	2.8	2.8	0.3
Arg^{18}(NH2)-A78(O1P)	80	3.1	3.4	1.0
Arg^{19}(NH1)-U95(O2P)	60	2.7	5.2	2.2
Arg^{19}(NH1)-A94(O1P)	60	2.7	4.7	1.8
Arg^{18}(NH1)-C93(O2P)	48	3.2	5.4	2.8
Gln^{75}(NE2)-U103(O2′)	38	3.1	4.0	1.2

The x-ray distances and the average MD distances along the whole trajectory supplemented by the standard deviations are stated in the table.

Arg^{18} with residues C92 and C93 were again restored after 18 ns (closed geometry).

The complex is stabilized by long-residency water bridges

We have detected a number of water-mediated contacts between the L25 protein and the RNA, most of them involving long-residency water molecules. We explicitly listed all long-residency hydration sites with residency times of individual water molecules longer than 1 ns and with 100% occupancy of hydration sites (Table 4). In both contact areas long-residing water molecules were identified in cavities formed between surfaces of the protein and the RNA. The averaged residency times of these water molecules ranged from 2 to 8 ns (Table 4) whereas at two hydration sites a single water molecule was bound with no exchange event in the course of the entire 24-ns simulation (Fig. 7). All water bridges listed in Table 4 are clearly visible in the x-ray structure except for the G79(O2P)-Lys14(NZ) water bridge. For a comparison, common hydration sites in nucleic acids have residency times on a scale of 0.05–0.5 ns (Nagan et al., 1999) whereas in our preceding studies of unbound LE motif (Reblova et al., 2003b) and (beet western yellows virus frame-shifting pseudoknot (Csaszar et al., 2001) we reported several highly structured hydration sites with residency times up to 5 ns. This study thus reveals water-residency times longer than any preceding MD analysis of nucleic acids.

TABLE 4 Water bridges between protein and RNA residues in the LE/HeIV-L25 complex (simulation COM1)

Residue(atom)	Averaged residency time (ns)	No. of distinct water molecules
First contact area		
G75(O2′)-Ala^{28}(O)-Arg^{9}(NH1)	24*	1
G75(N3)-U74(N3)-Asp^{90}(OD1)	8	3
G102(N2)-Asp^{90}(OD1)-Tyr^{31}(OH)	5	5
Second contact area		
G76(O2P)-U77(O2P)-G98(N1)-Lys^{14}(N)-Ser^{17}(OG) hydration pocket†	24*	1
G79(O2P)-Lys^{14}(NZ)	2	12
U77(O1P)-A78(O2P)-Arg^{18}(NE)	8	3

*In this site, a single water molecule is bound in the course of the simulation with no exchange event.

†The water is primarily bound to G76(O2P) and U77(O2P) while temporarily interacting with the remaining three atoms in the course of the simulation.

Hydration of L25 and LE/HeIV

There are additional major hydration sites outside the RNA-protein binding area. Table 5 summarizes L25 hydration sites with residency times of individual water molecules at least 3 ns. Long-residing water molecules stabilize adjacent secondary elements of the protein or loops between secondary elements (see Fig. S5 in Supplementary Material). For the LE/HeIV fragment we listed hydration sites with residency times >1 ns (Table 6). We observed two water-mediated basepairs, namely G75/A101 and G76/G100, in agreement with x-ray data (Correll et al., 1997). Both sites were 100% occupied with averaged water residency times 6 and 5 ns, respectively. In the G75/A101 basepair one long-residing water molecule was bound for 11 ns (Fig. 8) whereas in the G76/G100 basepair the longest water-binding event lasted 8 ns. This is a considerable prolongation of water binding compared to simulations of free LE where water residency

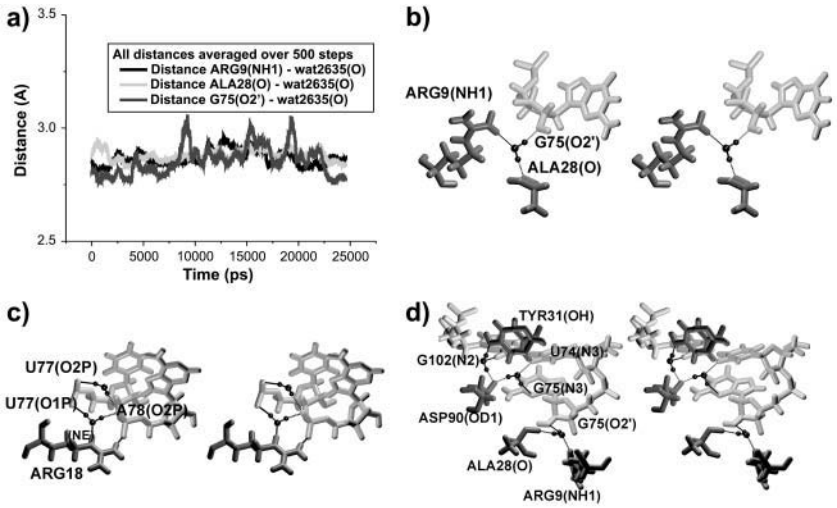

FIGURE 7 (*a*) Intermolecular RNA-protein contact (simulation COM1) mediated by a single water molecule bridging residues Arg^{9}, Ala^{28}, and G75 over the whole trajectory. (*b*) Stereo view of the Arg^{9}, Ala^{28}, and G75 water bridge. (*c*) Stereo view of the U77(O1P)-A78(O2P)-Arg^{18}(NE) hydration site and another proximal long-residing hydration site (see below) between U77(O2P) and A78(O2P). (*d*) Stereo view of the three intermolecular water bridges in the LE contact area. Amino acids are in dark gray, RNA residues are in gray, and water molecules are in black. Atoms forming water bridges are marked.

times in the same water-mediated basepairs were typically below 1 ns (Reblova et al., 2003b). A further hydration site was identified between U77(O2P) and A78(O2P) (Fig. 7 *c*) with averaged residency times of water molecules of 3 ns. Thus, the L25 binding leads to stabilization of long-residing water molecules, perhaps by reducing the flexibility of the RNA molecule.

The above hydration sites are clearly visible in the crystal structure, albeit the x-ray data do not provide any estimate of the timescale of the hydration exchange events. In comparison with simulations of free LE, long-residing hydration sites in A-stacks described earlier (Reblova et al., 2003b) are also occupied in the LE/HeIV-L25 complex, however, residency times of individual water molecules drop to ~0.5 ns. Furthermore, we observe a hydration site in the A99-A78 A-stack between G98(N2) and U77(O2P) with water-residency times up to 6 ns that was not seen in free LE.

TABLE 5 Long-residency water bridges in the protein structure

(se-wat-se)	(l-wat-l)	Residue(atom) involved	Averaged residency time (ns)	No. of distinct water molecules
β4 and β6		Ile^{63}(O)-Lys^{71}(N)-Val^{72}(N)	3	8
β6 and β7		Asp^{90}(OD1)-Asp^{76}(OD1)	3	8
	β2 and β3	Glu^{35}(O)-Lys^{32}(N)	5	5
α3 and β6		Phe^{56}(O)-Glu^{59}(O)-Ala^{74}(N)	6	4
	β6 and β7	His^{80}(NE2)-Leu^{86}(O)	4	6
	β1 and α1	Glu^{11}(O)-Arg^{9}(NE)	6	4

Long-residing water molecules bridge residues of adjacent secondary elements (se-wat-se) or residues in loops between secondary elements (l-wat-l). All water molecules with residency times >3 ns were analyzed. The number of single water molecules occupying the hydration site during the simulation is stated in the table (simulation COM1).

Long-residing water molecules seen in the A-stack region between G72(O6) and G102(O2P) in free LE (Reblova et al., 2003b) are not observed in the LE/HeIV-L25 complex. This site reveals only fractional hydration with residency times of individual water molecules 0.2–0.4 ns. The hydration pocket formed by A73(O2P), U103(O4), and G102(O6) in simulations of free LE (Reblova et al., 2003b) is also absent in the complex. It is because the A73(O2P)-U103(O4) distance increases from 4.5 Å to 7.7 Å after 3 ns of the simulation, which does not allow the hydration pocket to form. These differences clearly indicate that long-residency hydration sites are involved in stabilization of local conformational variations and substates of the biomolecule. Thus, the exact distribution of the long-residency hydration sites depends on the local architecture and is obviously affected by protein binding and presence of cations. It is to be noted that none of the listed long-residency hydration sites includes waters from the first hydration shell of Mg^{2+} cations.

Mg^{2+} and Na^{+} binding

The x-ray LE/HeIV-L25 complex contains five Mg^{2+} ions (marked as A–E) bound to the LE/HeIV fragment (Fig. 9). The ions A–D are bound in the major groove of LE whereas ion E is bound in the major groove of HeIV. Mg^{2+} ion A is bound to G106(O6, O2P) and G105(O2P) via outer-shell binding during the whole simulation. Mg^{2+} ion C is per-

TABLE 6 Long-residency hydration sites (bridges) in the LE/HeIV RNA

Residue(atom)	Averaged residency time (ns)	No. of distinct water molecules
G75(N1)-A101(N1)	6	4
G76(O6)-G100(N7)	5	5
U77(O2P)-A78(O2P)	3	8
G98(N2)-U77(O2P)	6	4

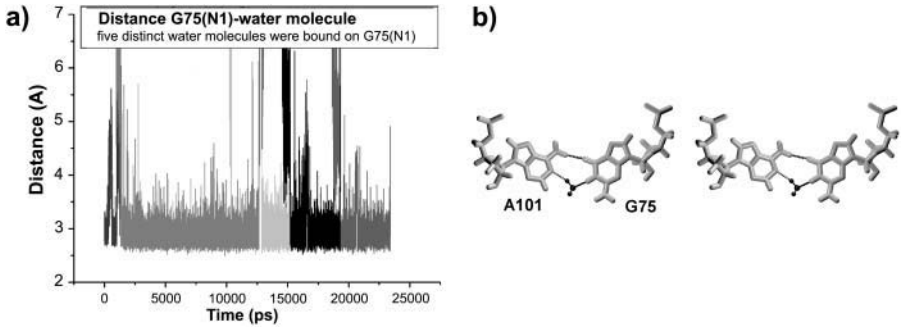

FIGURE 8 (*a*) Water bridges in the A101/G75 basepair in the course of COM1 simulation. Five distinct water molecules bridged A101(N1) and G75(N1) in the course of 24 ns. (*b*) Stereo view of the water-mediated A101/G75 basepair.

manently bound to G100(O2P) via inner-shell binding while Mg^{2+} ion D permanently binds the U74(O2P), G75(O2P), and A99(O2P) phosphate groups of the opposite strands via outer-shell binding. Mg^{2+} ion E permanently binds U95(O4) and G96(O6) via inner-shell binding. Mg^{2+} ions B and C are separated only by 3.3 Å in the x-ray structure (Fig. 9). Their distance increases up to 5.8 Å after equilibration and the Mg^{2+} ion B is released into the solvent after 8 ns of the simulation. After 20 ns of simulation, Mg^{2+} B bridges the G98(O2P) and C97(O2P) phosphate groups and the Gln^{12}(O) via outer-shell binding in the major groove of LE (Fig. 9). This binding remains stable until the end of the simulation. As discussed in the literature, the two x-ray ions B and C likely represent a single Mg^{2+} ion visiting two sites with fractional occupancies (Hermann and Patel, 1999). Thus, expulsion of one of the ions in the simulation is not surprising. We included both cations in the simulation to allow the system to select which of them is more stable.

In the course of the simulation we observed low occupancy of the RNA sites by Na^+ ions with the highest occupancy being only 31%. The criteria for Na^+-binding events have been described in our previous studies (Reblova et al., 2003b; Spackova et al., 2000) and imply inner-shell binding to a given atom. The most occupied positions by Na^+ ions were in the region close to the HeIV, namely at G84(N7) and G83(N7). Other Na^+-binding events were detected at the G72(O6, N7) position in LE with 12% occupancy. This rather insignificant Na^+ binding is not surprising considering the presence of several divalent cations in the most prominent cation-binding sites.

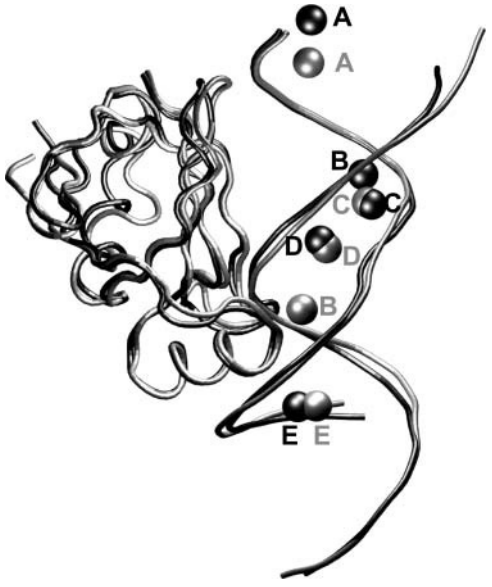

FIGURE 9 The x-ray LE/HeIV-L25 complex (*black*; NDB code, PR0018) and averaged MD structure (20–24 ns; *gray*) (simulation COM1) with five Mg^{2+} ions A–E.

Additional simulations

For a further assessment of the studied system we carried out additional simulations.

LE/HeIV-L25 complex in absence of Mg^{2+} shows no basepair perturbation

We performed simulation COM2 of the LE/HeIV-L25 complex in the absence of Mg^{2+} ions to study in detail the interaction of Na^+ ions with the LE/HeIV fragment and to investigate the influence of Mg^{2+} ions on the stability of the complex. The RMSD value of the complex with respect to the x-ray structure was 2.5 ± 0.4 Å (supplementary Fig. S1), i.e., the same as in simulation COM1 with Mg^{2+}.

All basepairs were stable including those at the LE/HeIV junction. This is a rather substantial difference compared to the simulation COM1. The major groove width of LE fluctuated in the range of 7–10 Å whereas the major groove of HeIV fluctuated in the range of 12–16 Å. The calculated groove width histograms (not shown) revealed a single substate for LE with the averaged value of 8.3 Å and also one substate for HeIV with the averaged value of 14.6 Å. Thus, the flexibility of the RNA appears to be modified by the removal of Mg^{2+} albeit the simulation may be too short to identify the HeIV substates. The LE region is definitely more flexible in the absence of Mg^{2+}.

Na^+ ions extensively bind in the major groove of LE in the course of the simulation (mostly to N7 and O2P atoms). Table 7 summarizes all Na^+-binding sites with occupancy ≥30% in the LE/HeIV fragment, the highest occupancy was 88% in LE at G102(N7) (Fig. 10). All these sites were

TABLE 7 Distribution of the main Na^+-binding positions along the LE/HeIV with occupancies ≥30% in the course of simulation COM2 of the LE/HeIV-L25 complex in the absence of Mg^{2+}

Na^+-binding positions in LE (atom) occupancy [no. of exchanged inner shell Na^+ ions]			
–	G106	C70	–
(N7) 44% [6]	G105	C71	–
–	A104	G72	(O6) 30% [9]
–	U103	A73	(O2P) 32% [9]
(N7) 88% [1]	G102	U74	–
(N7) 74% [2]	A101	G75	(N7) 77% [3]
(O2P) 38% [7]			
–	G100	G76	(N7) 68% [3]
			(O6) 30% [4]
(O2P) 42% [10]	A99	U77	–
–	G98	A78	–
–	C97	G79	–

observed in the LE region whereas Na^+-binding sites in the HeIV region showed occupancies <25%. One Na^+ site with occupancy 63% was observed at the Gln^{12}(O) in the protein structure. Other binding sites in protein show occupancy <15%.

All direct interactions involving amino acids and bases seen in the x-ray structure were observed in the LE/HeIV-L25 complex simulated in the absence of Mg^{2+} ions. These H-bonds were accompanied by other interactions between amino acids and sugar-phosphate backbone and as shown in Supplementary Material (Table S3), simulations COM1 and COM2 provide a close-to-identical picture of the direct RNA-protein interactions. We also analyzed hydration in the absence of Mg^{2+} and sites with water molecules residing 1 ns or more are given in Supplementary Material (Table S4). Six indirect water bridges between protein and RNA were observed. We again evidenced the hydration site G75(O2′)-Ala^{28}(O)-Arg^{9}(NH1) with one permanently bound water molecule, as in the COM1 simulation. Another hydration site Asp^{76}(OD2)-Asp^{90}(OD1)-G75(N2) with a permanently bound water molecule was not observed in the COM1 simulation, however, water-mediated contact between Asp^{76}(OD2) and G75(N2) was described by the x-ray study (Lu and Steitz, 2000). Furthermore, we identified two hydration sites that partly overlap with those seen in the COM1 simulation (supplementary Table S4 *a*). Thus, the long-residing hydration pattern is modified to a certain extent, which supports our conclusion above that in the complex molecules the exact position of long-residing water molecules is dependent quite significantly on the local structural variations. Long-residing water molecules were observed also in the LE/HeIV fragment outside the RNA-protein binding surface (supplementary Table S4 *b*). The two water-mediated G75/A101 and G76/G100 basepairs were again identified with 100% occupancy. The basepair G75/A101 revealed one permanently bound water molecule, the second G76/G100 basepair showed long-residing water molecules with residency times up to 2 ns. Other hydration sites in the LE/HeIV fragment were identified mainly between adjacent phosphates groups (supplementary Table S4 *b*), which is in reasonable agreement with the COM1 simulation. Long-residing water molecules observed in the protein structure again bridged residues of adjacent secondary elements or residues in loops between secondary elements.

Simulations of free RNA

The RNA molecule was further simulated in isolation assuming its structure from the RNA-protein x-ray complex as the starting geometry with inclusion of five crystallographic Mg^{2+} ions (simulation RNA1). The RMSD value with respect to the x-ray structure was 2.2 ± 0.6 Å (Fig. S1). The majority of the standard and the non-Watson-crick basepairs were stable over the entire simulation and were in agreement with the x-ray structure. The only exceptions were again two basepairs at the LE/HeIV junction. The G79=C97 basepair exhibited an opening event of the G79(N1)-C97(N3) and G79(O6)-C97(N4) H-bonds in the time period of 9.8–11.6 ns whereas the third G79(N2)-C97(O2) H-bond was stable. The U80/G96 basepair was essentially disrupted after equilibration, thus the H-bond between U80(N3) and G96(O6) was not formed. The basepair was stabilized by the U80(O2)-G96(N1) H-bond, showing an opening event in the time period of 9.2–9.5 ns.

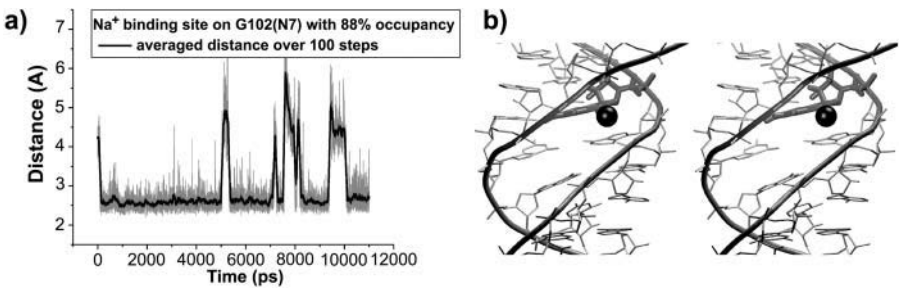

FIGURE 10 (*a*) The most prominent Na^+ inner-shell binding site at G102(N7) with 88% occupancy in the LE/HeIV-L25 complex simulated in the absence of Mg^{2+} ions. Note that the site is not occupied at the beginning of the simulation and although it involves only a single cation the binding is not continuous. The cation seems to be trapped in the very deep major groove and is not substantially interacting with other atoms except for G102(N7). No interaction with G102(O6) is seen. The other main Na^+-binding sites are visited by multiple cations. (*b*) Stereo view of the major groove of LE with Na^+ ion (*black*) bound at G102(N7) site (*dark gray*).

The geometry of the LE was in agreement with the x-ray structure of the complex. The LE major groove width fluctuated in the range of ~6–8 Å whereas the HeIV region showed considerable dynamics of the major groove with fluctuations in the range of 10–16 Å. This resembles the dynamics seen in the LE/HeIV-L25 complex during the simulation, however, no distinct substates of the major groove of HeIV were observed. Histograms for the major groove widths (data not shown) identified one substate for LE with average value 7.0 Å and one substate for HeIV with average value 14.6 Å. The simulated Mg^{2+}-binding sites were in agreement with x-ray positions except for the Mg^{2+} ion B. The x-ray distance between Mg^{2+} ions B and C is only 3.3 Å (see above) (Fig. 9). We observed redistribution of Mg^{2+} ions B and C, as in the COM1 simulation. After equilibration the distance increased to 5.7 Å. Mg^{2+} ion C remained bound to G100(O2P) via inner-shell binding while Mg^{2+} ion B was attached to G100(O1P), also via inner-shell binding. This binding persisted until the end of the simulation.

We observed water molecules in water-mediated G76/G100 basepair with residency times of 2–3 ns. The second water-mediated G75/A101 basepair shows residency times of individual water molecules in the range of 0.5–0.8 ns. Another long-residing water molecule binds simultaneously G102(O6) and a water molecule from the first water shell of Mg^{2+} ion D that interacts with U75(O2P) via inner-shell binding. The water molecule thus bridges G102(O6) and the hydrated Mg^{2+} ion D for 12 ns and then is replaced by another water molecule. Another hydration site was observed between U103(O4) and G102(O6) with one long-residing water molecule bound for 8 ns of the simulation; residency times of other water molecules in this site ranged from 0.8 to 2 ns.

The x-ray structure of the free LE/HeIV fragment (Correll et al., 1997) with a wide (open) HeIV major groove was used as the starting structure in another simulation RNA2 (see Materials and Methods) (Fig. 3 *b*). Five Mg^{2+} ions used in this simulation are in a similar but not identical arrangement compared with the LE/HeIV-L25 complex (see Materials and Methods).

The RMSD value with respect to the starting x-ray structure was 2.2 ± 0.5 Å (supplementary Fig. S1). All basepairs were entirely stable except for the A73/U103 basepair from the first A-stack of LE. This basepair exhibited one opening event in the time period of 2.3–3.2 ns. Both A73(N6)-U103(O2) and A73(N7)-U103(N3) H-bonds were temporarily disrupted, however, the basepair formed again. It is noted that a similar fluctuation in the A77/U99 basepair in the second A-stack was previously reported (Reblova et al., 2003b) and this indicates that the basepairs involved in the A-stack arrangements may be somewhat labile.

We observed minor fluctuations of the major groove width of LE (scale of fluctuations ~1–2 Å). The Mg^{2+} ions bridge opposite phosphates across the major groove of LE, stabilizing its width. The major groove of HeIV showed substantial fluctuations in the range of 11–19 Å. Histograms identified one substate for LE with the averaged width value of 6.5 Å whereas two substates were found for HeIV with the averaged values of 12.7 Å (closed geometry) and 17.0 Å (open geometry), similar to the COM1 simulation. Mg^{2+} cations did not change binding positions after equilibration and in the course of 18 ns of the simulation (Table 2). Mg^{2+} C linked the opposite phosphate groups U74(O2P) and A99(O2P) via inner-shell binding, which considerably narrowed the major groove of LE. The simulation revealed two hydration sites with long-residing water molecules with the range of binding times of 1.5–2 ns. Further, we identified two water-mediated basepairs G76/G100 and G75/A101. The first one showed water molecules with residency times up to 5 ns whereas the second one was characterized by hydration events in the range of 0.5–0.8 ns, in agreement with our previous study of smaller free LE (Reblova et al., 2003b).

Simulations of free protein reveal reduced stability of helix-α1

We carried out simulation PROT1 of the L25 protein (starting from the crystal structure of the complex) in the absence of the LE/HeIV fragment. During 10 ns of simulation the structure of the protein was stable. The RMSD value with respect to the x-ray structure was 2.3 ± 0.4 Å (Fig. S1). The RMSD values of the individual secondary elements with respect to the x-ray structure were in the range of 0.3–0.5 Å and no structural or dynamic changes were observed. In contrast, the elevated temperature (400 K) simulation (PROT2) resulted in RMSD value with respect to the x-ray structure of 5.6 ± 1.3 Å (Fig. S1). The most significant

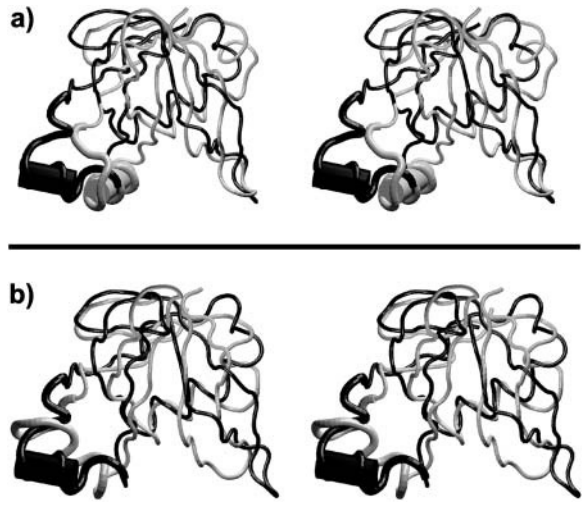

FIGURE 11 (*a*) X-ray structure of complexed L25 protein (*gray*) (NDB code, PR0018) superimposed with the averaged MD structure (18–19 ns) during the 400-K simulation (*black*); the helix-α1 is represented as cylinder. (*b*) NMR structure (PDB code, 1B75) of free L25 protein (*gray*) superimposed with the 400-K averaged MD structure.

changes were observed for helix-α1 (Fig. 11) showing two gradual rearrangements. First, the helix-α1 underwent a partial disruption of its helical secondary structure producing the highest RMSD value for a single helix (1.6 Å) with respect to the x-ray structure. Other secondary elements showed RMSD values in the range of 0.5–1.0 Å. The second change of helix-α1 can be characterized as a rigid-body rotation by ~90° (Fig. 11 *a*). The simulation thus indicates that the helix-α1 is the most flexible and dynamical part of the protein. No additional significant structural or dynamical changes were detected in the other secondary structure elements.

DISCUSSION

RNA-protein interactions and tightly bound water molecules

The ribosomal RNA-protein LE/HeIV-L25 complex from *E. coli* has been investigated utilizing MD simulations, extending several previous studies dealing with free LE (Auffinger et al., 2004a; Reblova et al., 2003b). MD simulations were carried out on x-ray structures of the complex and free RNA (Correll et al., 1997; Lu and Steitz, 2000). The complex was simulated assuming the x-ray structure as the starting geometry in the presence and in the absence of Mg^{2+} cations. Further, simulations of individual components of the complex were carried out and the x-ray structure of the free LE/HeIV fragment was simulated (Correll et al., 1997).

In agreement with the x-ray data all five intermolecular H-bonds between amino acids and bases were observed, namely G75(N2)-Asp^{90}(OD2), G76(N3)-Gln^{78}(NE2), G98(O6)-Lys^{14}(N), U80(O4)-Lys^{14}(NZ), and G79(N7)-Lys^{14}(NZ) (Table 3), albeit some of them with fractional occupancies. Intermolecular H-bonds between amino acids and bases occur in two contact areas (LE and HeIV) and are accompanied by multiple H-bonds between amino acids and sugar-phosphate backbone (Table 3). These H-bonds are also in reasonable agreement with the x-ray structure, although some of them fluctuate. The electrostatic interactions significantly contribute to the stability of the LE/HeIV-L25 complex (Table S2), which has been shown before for other RNA-protein complexes (Guo and Gmeiner, 2001). The van der Waals interactions are not significant, probably due to the absence of bulged-out bases that could stack with aromatic amino acids. The overall agreement with the x-ray structure is good though not perfect, as demonstrated by considerable fluctuations of certain H-bonds (see above). All five direct intermolecular contacts between amino acids and bases were also preserved in the simulation of the complex in absence of the x-ray Mg^{2+} ions. Also the agreement for direct contacts between amino acids and sugar-phosphate backbone was very good and both simulations are qualitatively consistent with the x-ray structure. The stability of the LE/HeIV-L25 complex in the absence of Mg^{2+} ions was thus not perturbed on this simulation timescale.

The simulations revealed multiple water bridges in the LE/HeIV-L25 complex, involving long-residency water molecules with binding times ranging from 2 to 24 ns (Table 4). Two of the water molecules were bound through the entire simulation with no exchange event. For a comparison, water molecules in common hydration sites in nucleic acids have binding times 0.05–0.5 ns whereas specific long-residency hydration sites with water-binding times of 1–5 ns were reported recently for several nucleic acid systems (Csaszar et al., 2001; Guo and Gmeiner, 2001; Nagan et al., 1999; Reblova et al., 2003b; Schneider et al., 2001; Spackova et al., 2000, 2003). Additional long-residency hydration sites were found around the protein and around the LE/HeIV RNA outside the RNA-protein contact area (Tables 5 and 6). The two water-mediated G75/A101 and G76/G100 LE basepairs show averaged water-residency times of 6 and 5 ns. This means a substantial prolongation of the water-residency times compared to simulations of isolated LE (Reblova et al., 2003b), where the residency times were $<$1 ns, in agreement with other simulations of water-mediated RNA basepairs carried out so far (Brandl et al., 2000; Schneider et al., 2001). In summary, this work identifies the longest residency times for individual water molecules reported so far for nucleic acids. We evidenced several important hydration sites also in simulation of free LE/HeIV fragment, albeit not as significant as in the complex (cf. also Reblova et al., 2003b). Thus we suggest that long-residency hydration sites represent an important element of the three-dimensional structure of rRNA. Interestingly, some of the presently observed long-residency hydration sites do not overlap with those identified in solution simulations of free LE molecule (Reblova et al., 2003b). This could suggest that at least some long-residency hydration sites are substantially affected by local conformational variations of the solute molecule and are in fact involved in the delicate balance of substates of the solute structure (Reblova et al., 2003b; Spackova et al., 2000, 2003). Then, upon quite subtle changes of the solute geometry, some long-residency hydration sites may convert into common fast-exchange hydration sites, shift to nearby positions, or disappear entirely. On the other hand new long-residency sites may emerge. Comparison of the presently available trajectories indicates examples of all such scenarios. It is in addition rather apparent that when extending the simulated system from free RNA to RNA-protein complex the timescale of hydration events increases. This is due to presence of more complex solute architecture with additional water bridges or hydration pockets as well as possibly due to reduced flexibility of the RNA molecule upon the protein binding. Thus the water-residency times are likely to further increase inside larger biomolecular assemblies such as the ribosomes where some water molecules may be bound almost permanently. The long-residency water molecules may be involved in regulation of conformational substates

and dynamical motions. Nevertheless, caution is still needed regarding the above assessment of the long-residency hydration events. First, in most cases our analysis is based on a single trajectory on each system and on a comparison of several related trajectories. Thus quantitative reproducibility of long-residency hydration states could not be achieved and the discussion is based rather on observing a few ''snapshots'' of the long-residency hydration architecture. Second, formation of many long-residency sites (typically those involving the formation of ''cavities'') may be associated with restricted diffusion and thus accompanied with an entropic cost. Therefore, it is presently not possible to quantify the actual effect of long-residency hydration on the stability of the complex.

Cation binding in the LE/HeIV-L25 complex

The x-ray structure of the LE/HeIV-L25 complex contains five Mg^{2+} ions bound via inner- and outer-shell binding in the RNA deep major groove. Mg^{2+} ions did not change binding positions in the course of the simulation and were in agreement with the x-ray positions, except for Mg^{2+} ion B. In the x-ray structure Mg^{2+} cations B and C are separated by only 3.3 Å (Fig. 9). It is well established that the B- and C-binding positions likely represent a single cation-binding site with fractional occupancy (Hermann and Patel, 1999). In the course of simulation, Mg^{2+} C stayed in place whereas Mg^{2+} ion B was expelled from its original position and then occupied a new position in the major groove. As discussed by other groups, many x-ray positions of Mg^{2+} cations do not reflect the biologically important cations and some unrelated electron densities (anions, water) can even be misinterpreted as cations (Auffinger et al., 2004b; Ennifar et al., 2003). Similar redistribution of the Mg^{2+} ions in the major groove of LE has been also observed in our previous study (Reblova et al., 2003b). On the other hand, it is fair to note that modeling of divalent cations suffers from major limitations imposed by the pair-additive force field, making the description of the interactions of divalent cations the least accurate part of the simulations. In reality, there are huge polarization and charge-transfer effects from the cation to all its first-shell ligands, further propagating well beyond the first ligand shell (Gresh et al., 2003; Rulisek and Sponer, 2003). For example, properties of the first-shell water molecules are substantially different from bulk water molecules. Furthermore, the simulations are orders of magnitude shorter compared with a timescale that would be appropriate for a representative sampling of motions of divalent cations. Thus, the results of this simulation and related such studies should be considered primarily as crude estimates of the effect of Mg^{2+} ions bound in the suggested x-ray positions. It is not possible to exactly localize the preferred Mg^{2+} positions and binding patterns via contemporary MD simulations and even their interactions in known x-ray sites may be biased by the force-field limitations. The force-field and sampling limitations actually justify the common practice in the majority of simulations of nucleic acids where the counterion atmosphere is simply described by a minimal neutralizing set of monovalent cations. (Inclusion of monovalent anions such as Cl^- into the simulation is more risky as the force field for anions has not been widely tested and the pair-additive force fields are inherently deficient in describing the anions due to the diffuse nature of their electron distributions (Tobias et al., 2001)). Fortunately, because the simulations are too short to lead to any substantial RNA unfolding due to the absence of the Mg^{2+} species, lack of divalent cations in simulations has a much smaller effect than it has on experiments.

The description of the monovalent cation interactions with nucleic acids is considerably better although not perfect. We carried out the simulations in the presence of Na^+ cations rather than in the presence of the physiologically more relevant K^+ ones because there is currently considerably more experience with the behavior of sodium simulations in the MD literature. Anyway, description of both cations is affected by the same force-field approximations. In the course of simulation with Mg^{2+} no strong Na^+-binding events were observed. However, the simulated LE/HeIV-L25 complex in the absence of Mg^{2+} reveals extensive binding of Na^+ ions mostly with multiple exchange events of the cations (Table 7). The most occupied sites were found in the major grove of LE with maximal occupancy of one site reaching as much as 88% (Fig. 10). The most occupied atoms were N7 and O2P. The area of HeIV shows low Na^+ binding with the maximal occupancy in an individual site of 25%. Thus the simulation confirms that the major groove of LE provides some of the most prominent RNA cation-binding sites studied to date (Auffinger et al., 2004a; Correll et al., 1997; Reblova et al., 2003b).

Basepairing

The simulation of the LE/HeIV-L25 complex in the presence of x-ray Mg^{2+} ions reveals that the standard and non-Watson-Crick basepairs are stable and in agreement with the x-ray structure, except for the three consecutive basepairs (Watson-Crick G79=C97, wobble U80/G96, and wobble G81/U95) forming the LE/HeIV junction. The first basepair shows two opening events, the second basepair is essentially disrupted, and the third basepair shows fluctuation of one H-bond. Interestingly, all basepairs are entirely stable when the LE/HeIV-L25 complex is simulated in the absence of Mg^{2+} ions whereas Mg^{2+} simulation of the free LE/HeIV fragment (in the absence of the L25 protein) reveals again instability of the G79=C97 and U80/G96 basepairs. In contrast, all basepairs are stable in another Mg^{2+} simulation of free LE/HeIV with somewhat different Mg^{2+} distribution (see Materials and Methods). When considering all data we suggest that the destabilization of the LE/HeIV junction basepairs might be related to the presence of the Mg^{2+} ion E bound to both wobble basepairs, specifically to positions

U95(O4) and G96(O6). It is not possible to decide whether this reflects some error in the initial (or experimental) cation placement, force-field limitation, or insufficient sampling (see Discussion above). It also cannot be ruled out that actually the junction between the LE and HeIV regions may be the most labile part of the RNA molecule. For example, the instability of the basepairs at the LE/HeIV junction could also be partly related to the cross-strand G81/G96 stack. Stacking interactions can lead to basepair strain that can result in modest instability of the basepairing or opening events. Actually, occasional temporary opening events of A/U basepairs were noticed also in the LE A-stacks; see above and Reblova et al. (2003b). Nevertheless, the perturbation of the LE/HeIV junction most likely stems from the limitations (artifacts) related to inclusion of divalent cations into simulations. Because the instability at the LE/HeIV junction did not have any significant effect on the protein binding it was not necessary to repeat the simulations.

The protein dynamics

L25 protein in the LE/HeIV-L25 complex underwent no significant structural and dynamic changes in the course of simulation. Modest rotation of the helix-α2 was noticed compared with the starting geometry (supplementary Figs. S2 and S3). This change did not influence the stability of the LE/HeIV-L25 complex. No additional structural changes were detected. Simulations of isolated L25 protein (starting from its geometry in the complex) at 300 K and 400 K reveal the following picture. There were no structural changes during the 300-K simulation. At elevated temperature (400 K), substantial structural changes were observed in the helix-α1. The helix-α1 rotated by $\sim$90° and its secondary structure was partially disrupted (Fig. 11). Interestingly, this observation is in a full agreement with the experimental studies (Stoldt et al., 1998, 1999) showing that formation of the RNA-protein complex induces structuring of the helix-α1 region that turns toward the major groove of HeIV. Our simulation of the L25 protein at elevated temperature could, at least qualitatively, capture a reversal of this process. After 19 ns of simulation at elevated temperature, the protein structure resembles the solution NMR structure of free L25 protein (Fig. 11 *b*) (Stoldt et al., 1998).

Dynamics of the LE/HeIV explains the differences between experimental structures

Different nanosecond dynamic behavior has been observed for the LE and HeIV motifs. The LE region is very rigid whereas the HeIV segment shows considerable dynamics. Two substates (open and closed geometry) of the major groove of HeIV have been observed for both complexed and free LE/HeIV fragments in the simulations (Figs. 4 and 5). Both substates were also observed in the experimental structures (Correll et al., 1997; Lu and Steitz, 2000; Stoldt et al., 1999). The ''open geometry'' is seen in the x-ray structure of free LE/HeIV RNA duplex (Correll et al., 1997) and also in the NMR LE/HeIV-L25 complex (Stoldt et al., 1999) (Fig. 3, *b* and *c*) whereas the closed geometry is seen in the x-ray LE/HeIV-L25 complex (Lu and Steitz, 2000) (Fig. 3 *a*).

Clear substates of the major groove of HeIV were not identified in the LE/HeIV-L25 complex in the absence of Mg^{2+} ions; nevertheless, major grooves of both LE and HeIV considerably oscillated. The major groove of LE showed fluctuations in the range of 7–10 Å, probably due to the absence of the Mg^{2+} ions in the major groove (Reblova et al., 2003b). It has no effect on the RNA-protein binding. The major groove of HeIV showed breathing in the width range of 12–16 Å. In summary, both complexed and free LE/HeIV rRNA reveal considerable dynamics in the area of HeIV on the nanosecond timescale. Notably, the NMR and x-ray structures of the LE/HeIV-L25 complex show differences primarily in the HeIV area (Fig. 3). We suggest that the differences can be explained by our MD simulations that identify the HeIV as a flexible RNA fragment with variable width of the major groove, likely sensitive to the molecular interactions and environmental effects.

CONCLUSIONS

We have carried out a series of MD simulations to study the complex between *E. coli* loop E/helix IV 5S rRNA fragment and ribosomal protein L25. Although the exact biological role of this complex is yet to be determined (L25 could, for example, play a role in supporting the *E. coli* loop E so it can interact with the A-site finger) it is well characterized by atomic resolution experimental techniques and reveals very interesting molecular interactions (Lu and Steitz, 2000; Stoldt et al., 1999). There is a very good overall agreement between the experimental and simulated structures, which is quite promising considering further studies of RNA-protein interactions. Nevertheless, some minor differences between computed and experimental structures were observed (see above) and these might be attributed to force-field limitations and possibly data and refinement errors in the experimental structures. They involve temporary oscillations (fractional occupancy) of some of the direct RNA-protein H-bonds and perturbations of basepairs at the LE/HeIV junction in some simulations. This basepair instability has no effect on the L25 binding. The simulations strongly suggest that this RNA structural perturbation is caused by a divalent Mg^{2+} cation present in the area, highlighting the difficulties that are inherent to simulations with divalent cations. Their inclusion represents a controversial part of the contemporary simulation techniques, as neither the force field nor the sampling is satisfactory for realistic modeling of Mg^{2+}.

The simulations confirm that the deep major groove of LE is a prominent rRNA cation-binding site. In the absence of divalent cations, this part of RNA extensively binds

monovalent cations via inner-shell binding. The divalent cations rigidify the LE major groove geometry. The HeIV region shows clear bistability of its major groove width that is sensitive to the presence of cations and molecular interactions. Two HeIV substates, closed and open, were identified by the simulations. This nicely explains the observed difference between various HeIV experimental structures (Lu and Steitz, 2000; Stoldt et al., 1999). In agreement with the experimental data (Stoldt et al., 1998) the simulations suggest that helix-α1 of L25 is the least stable part of the protein that actually is structured upon the formation of the complex with rRNA.

The simulations reveal that the rRNA-protein interaction is mediated by a number of highly specific hydration sites with long-residing water molecules, two of them bound during the 24-ns simulation with no exchange event. Such water-binding events are approximately two orders of magnitude longer compared to water binding in common hydration sites around standard DNA and RNA duplexes. Long-residing water molecules are seen also outside the RNA-protein contact areas and the water-binding times are substantially enhanced compared to simulations of free RNA. Long-residency hydration sites thus represent important elements of the three-dimensional structure of rRNA and we suggest that inside the ribosome some of the water molecules can be bound almost permanently. MD simulations offer an important tool to study long-residency hydration sites in complex RNA systems because the available experimental methods only rarely reveal the timescale of the hydration events (Kochoyan and Leroy, 1995). However, substantial extension of the simulation timescale will be very vital to obtain a statistically complete and reproducible picture of the long-residency hydration events in rRNA.

SUPPLEMENTARY MATERIAL

An online supplement to this article can be found by visiting BJ Online at http://www.biophysj.org.

This work was supported by grants Ministry of Education, Youth and Sports, Czech Republic (LN00A016, the Wellcome Trust International Senior Research Fellowship in Biomedical Science in Central Europe (GR067507), and the National Institutes of Health (grants 2R15 GM55898 and 3R15 GM55898).

REFERENCES

Agalarov, S. C., G. S. Prasad, P. M. Funke, C. D. Stout, and J. R. Williamson. 2000. Structure of the S15,S18-rRNA complex: assembly of the 30S ribosome central domain. *Science*. 288:107–112.

Auffinger, P., L. Bielecki, and E. Westhof. 2003. The Mg^{2+} binding sites of the 5S rRNA loop E motif as investigated by molecular dynamics simulations. *Chem. Biol.* 10:551–561.

Auffinger, P., L. Bielecki, and E. Westhof. 2004a. Symetric K^{+} and Mg^{2+} ion-binding sites in the rRNA loop E inferred from molecular dynamics simulations. *J. Mol. Biol.* 335:555–571.

Auffinger, P., L. Bielecki, and E. Westhof. 2004b. Anion binding to nucleic acids. *Structure*. 12:379–388.

Auffinger, P., and E. Westhof. 1998. Simulations of the molecular dynamics of nucleic acids. *Curr. Opin. Struct. Biol.* 8:227–236.

Auffinger, P., and E. Westhof. 1999. Singly and bifurcated hydrogen-bonded base-pairs in tRNA anticodon hairpins and ribozymes. *J. Mol. Biol.* 292:467–483.

Ban, N., P. Nissen, J. Hansen, P. B. Moore, and T. A. Steitz. 2000. The complete atomic structure of the large ribosomal subunit at 2.4 A resolution. *Science*. 289:905–920.

Beaurain, F., and M. Laguerre. 2003. MD studies of the DIS/DIS kissing complex solution and x-ray structures. *Oligonucleotides*. 13:501–514.

Brandl, M., M. Meyer, and J. Suhnel. 2000. Water-mediated base pairs in RNA. A quantum-chemical study. *J. Phys. Chem.* 104:11177–11187.

Cheatham III, T. E., and M. A. Young. 2000. Molecular dynamics simulation of nucleic acids: successes, limitations, and promise. *Biopolymers*. 56:232–256.

Cornell, W. D., P. Cieplak, C. I. Bayly, I. R. Gould, K. M. Merz, D. M. Ferguson, Jr., D. C. Spellmeyer, T. Fox, J. W. Caldwell, and P. A. Kollman. 1995. A 2nd generation force-field for the simulation of proteins, nucleic-acids, and organic molecules. *J. Am. Chem. Soc.* 117:5179–5197.

Correll, C. C., B. Freeborn, P. B. Moore, and T. A. Steitz. 1997. Metals, motifs, and recognition in the crystal structure of a 5S rRNA domain. *Cell*. 91:705–712.

Csaszar, K., N. Spackova, R. Stefl, J. Sponer, and N. B. Leontis. 2001. Molecular dynamics of the frame-shifting pseudoknot from beet western yellows virus: The role of non-Watson-Crick base-pairing, ordered hydration, cation binding and base mutations on stability and unfolding. *J. Mol. Biol.* 313:1073–1091.

Ennifar, E., P. Walter, and P. Dumas. 2003. A crystallographic study of the binding of 13 metal ions to two related RNA duplexes. *Nucleic Acids Res.* 31:2671–2682.

Ferrin, T. E., C. C. Huang, L. E. Jarvis, and R. Langridge. 1988. The MIDAS display system. *J. Mol. Graph.* 6:13–27.

Gresh, N., J. E. Sponer, N. Spackova, J. Leszczynski, and J. Sponer. 2003. Theoretical study of binding of hydrated Zn(II) and Mg(II) cations to 5′-guanosine monophosphate. Toward polarizable molecular mechanics for DNA and RNA. *J. Phys. Chem. B*. 107:8669–8681.

Guo, J. X., and W. H. Gmeiner. 2001. Molecular dynamics simulation of the human U2B″ protein complex with U2 snRNA hairpin IV in aqueous solution. *Biophys. J.* 81:630–642.

Harms, J., F. Schluenzen, R. Zarivach, A. Bashan, S. Gat, I. Agmon, H. Bartels, F. Franceschi, and A. Yonath. 2001. High resolution structure of the large ribosomal subunit from a mesophilic Eubacterium. *Cell*. 107:679–688.

Harvey, S. C., R. K. Z. Tan, and T. E. Cheatham, Iii. 1998. The flying ice cube: velocity rescaling in molecular dynamics leads to violation of energy equipartition. *J. Comput. Chem.* 19:726–740.

Hermann, T., P. Auffinger, and E. Westhof. 1998. Molecular dynamics investigations of hammerhead ribozyme RNA. *Eur. Biophys. J.* 27:153–165.

Hermann, T., and D. J. Patel. 1999. Stitching together RNA tertiary architectures. *J. Mol. Biol.* 294:829–849.

Humphrey, W., A. Dalke, and K. Schulten. 1996. VMD - Visual molecular dynamics. *J. Mol. Graph.* 14:33–38.

Kochoyan, M., and J. L. Leroy. 1995. Hydration and solution structure of nucleic-acids. *Curr. Opin. Struct. Biol.* 5:329–333.

Leontis, N. B., J. Stombaugh, and E. Westhof. 2002. The non-Watson-Crick base pairs and their associated isostericity matrices. *Nucleic Acids Res.* 30:3497–3531.

Leontis, N. B., and E. Westhof. 1998a. The 5S rRNA loop E: chemical probing and phylogenetic data versus crystal structure. *RNA*. 4:1134–1153.

Leontis, N. B., and E. Westhof. 1998b. Conserved geometrical base-pairing patterns in RNA. *Q. Rev. Biophys.* 31:399–455.

Leontis, N. B., and E. Westhof. 2003. Analysis of RNA motifs. *Curr. Opin. Struct. Biol.* 13:300–308.

Lu, M., and T. A. Steitz. 2000. Structure of Escherichia coli ribosomal protein L25 complexed with a 5S rRNA fragment at 1.8-angstrom resolution. *Proc. Natl. Acad. Sci. USA.* 97:2023–2028.

Moore, P. B. 1999. Structural motifs in RNA. *Annu. Rev. Biochem.* 68:287–300.

Nagan, M. C., S. S. Kerimo, K. Musier-Forsyth, and C. J. Cramer. 1999. Wild-type RNA microhelix(Ala) and 3:70 variants: molecular dynamics analysis of local helical structure and tightly bound water. *J. Am. Chem. Soc.* 121:7310–7317.

Nevskaya, N., S. Tishchenko, R. Fedorov, S. Al-Karadaghi, A. Liljas, A. Kraft, W. Piendl, M. Garber, and S. Nikonov. 2000. Archaeal ribosomal protein L1: the structure provides new insights into RNA binding of the L1 protein family. *Structure.* 8:363–371.

Nikulin, A., I. Eliseikina, S. Tishchenko, N. Nevskaya, N. Davydova, O. Platonova, W. Piendl, M. Selmer, A. Liljas, D. Drygin, R. Zimmermann, M. Garber, and S. Nikonov. 2003. Structure of the L1 protuberance in the ribosome. *Nat. Struct. Biol.* 10:104–108.

Norberg, J., and L. Nilsson. 2002. Molecular dynamics applied to nucleic acids. *Acc. Chem. Res.* 35:465–472.

Orozco, M., A. Perez, A. Noy, and F. J. Luque. 2003. Theoretical methods for the simulation of nucleic acids. *Chem. Soc. Rev.* 32:350–364.

Pearlman, D. A., D. A. Case, J. W. Caldwell, W. S. Ross, T. E. Cheatham III, and S. DeBolt. 1995. AMBER, a package of computer programs for applying molecular mechanics, normal mode analysis, molecular dynamics and free energy calculations to simulate the structural and energetic properties of molecule. *Comput. Phys. Commun.* 91:1–41.

Perederina, A., N. Nevskaya, O. Nikonov, A. Nikulin, P. Dumas, M. Yao, I. Tanaka, M. Garber, G. Gongadze, and S. Nikonov. 2002. Detailed analysis of RNA-protein interactions within the bacterial ribosomal protein L5/5S rRNA complex. *RNA.* 8:1548–1557.

Reblova, K., N. Spackova, J. E. Sponer, J. Koca, and J. Sponer. 2003a. Molecular dynamics simulations of RNA kissing-loop motifs reveal structural dynamics and formation of cation-binding pockets. *Nucleic Acids Res.* 31:6942–6952.

Reblova, K., N. Spackova, R. Stefl, K. Csaszar, J. Koca, N. B. Leontis, and J. Sponer. 2003b. Non-Watson-Crick basepairing and hydration in RNA motifs: molecular dynamics of 5S rRNA loop E. *Biophys. J.* 84:3564–3582.

Ross, W. S., and C. C. Hardin. 1994. Ion-induced stabilization of the G-DNA quadruplex: free-energy perturbation studies. *J. Am. Chem. Soc.* 116:6070–6080.

Rulisek, L., and J. Sponer. 2003. Outer-shell and inner-shell coordination of phosphate group to hydrated metal ions (Mg^{2+}, Cu^{2+}, Zn^{2+}, Cd^{2+}) in the presence and absence of nucleobase. The role of nonelectrostatic effects. *J. Phys. Chem. B.* 107:1913–1923.

Sarzynska, J., T. Kulinski, and L. Nilsson. 2000. Conformational dynamics of a 5S rRNA hairpin domain containing loop D and a single nucleotide bulge. *Biophys. J.* 79:1213–1227.

Schneider, C., M. Brandl, and J. Suhnel. 2001. Molecular dynamics simulation reveals conformational switching of water-mediated uracil-cytosine base-pairs in an RNA duplex. *J. Mol. Biol.* 305:659–667.

Spackova, N., I. Berger, and J. Sponer. 2000. Nanosecond molecular dynamics of zipper-like DNA duplex structures containing sheared G.A mismatch pairs. *J. Am. Chem. Soc.* 122:7564–7572.

Spackova, N., T. E. Cheatham III, F. Ryjacek, F. Lankas, L. V. Meervelt, P. Hobza, and J. Sponer. 2003. Molecular dynamics simulations and thermodynamics analysis of DNA-drug complexes. Minor groove binding between 4′,6-diamidino-2-phenylindole (DAPI) and DNA duplexes in solution. *J. Am. Chem. Soc.* 125:1759–1769.

Sponer, J., H. A. Gabb, J. Leszczynski, and P. Hobza. 1997. Base-base and deoxyribose-base stacking interactions in B-DNA and Z-DNA: a quantum-chemical study. *Biophys. J.* 73:76–87.

Stoldt, M., J. Wohnert, M. Gorlach, and L. R. Brown. 1998. The NMR structure of Escherichia coli ribosomal protein L25 shows homology to general stress proteins and glutaminyl-tRNA synthetases. *EMBO J.* 17:6377–6384.

Stoldt, M., J. Wohnert, O. Ohlenschlager, M. Gorlach, and L. R. Brown. 1999. The NMR structure of the 5S rRNA E-domain-protein L25 complex shows preformed and induced recognition. *EMBO J.* 18:6508–6521.

Tobias, D. J., P. Jungwirth, and M. Parrinello. 2001. Surface solvation of halogen anions in water clusters: an ab initio molecular dynamics study of the $Cl^-(H_2O)_6$ complex. *J. Chem. Phys.* 114:7036–7044.

Vallurupalli, P., and P. B. Moore. 2003. The solution structure of the loop E region of the 5 S rRNA from spinach chloroplasts. *J. Mol. Biol.* 325: 843–856.

van der Spoel, D., A. R. van Buuren, E. Apol, P. J. Maulenhoff, P. D. Tieleman, A. L. T. M. Sijbers, B. Hess, K. A. Feenstra, E. Lindhal, R. V. Drunen, and H. J. C. Berendsen. 1999. Gromacs User Manual Version 2.0. Groningen, The Netherlands.

Wimberly, B. T., D. E. Brodersen, W. M. Clemons, R. J. Morgan-Warren, A. P. Carter, C. Vonrhein, T. Hartsch, and V. Ramakrishnan. 2000. Structure of the 30S ribosomal subunit. *Nature.* 407:327–339.

Wimberly, B. T., R. Guymon, J. P. McCutcheon, S. W. White, and V. Ramakrishnan. 1999. A detailed view of a ribosomal active site: the structure of the L11-RNA complex. *Cell.* 97:491–502.

York, D. M., T. A. Darden, and L. G. Pedersen. 1993. The effect of long-range electrostatic interactions in simulations of macromolecular crystal: a comparison of the Ewald and truncated list methods. *J. Chem. Phys.* 99:8345–8348.

Yusupov, M. M., G. Z. Yusupova, A. Baucom, K. Lieberman, T. N. Earnest, J. H. D. Cate, and H. F. Noller. 2001. Crystal structure of the ribosome at 5.5 angstrom resolution. *Science.* 292:883–896.

Zacharias, M. 2000. Simulation of the structure and dynamics of nonhelical RNA motifs. *Curr. Opin. Struct. Biol.* 10:311–317.

Zhou, R., B. J. Berne, and R. Germain. 2001. The free energy landscape for beta hairpin folding in explicit water. *Proc. Natl. Acad. Sci. USA.* 18:14931–14936.